The LASI High-Frequency Electromagnetic Subsurface-Imaging System

System Description and Demonstration Site-Characterization Survey at the Idaho National Engineering Laboratory

Ben K. Sternberg (BKS@MGE.ARIZONA.EDU; 602-621-2439)
Mary M. Poulton (MARY@MGE.ARIZONA.EDU; 602-621-8391)
Laboratory for Advanced Subsurface Imaging (LASI)
Dept. of Mining & Geological Engineering
Mines Bldg. #12, Room 229
University of Arizona
Tucson, AZ 85721

Abstract

A high-frequency, high-resolution, electromagnetic (EM) imaging system has been developed for environmental geophysics surveys. Some key features of this system include: (1) rapid surveying to allow dense spatial sampling over a large area, (2) high-accuracy measurements which are used to produce a high-resolution image of the subsurface, (3) measurements which have excellent signal-to-noise ratio over a wide bandwidth (31 kHz to 32 MHz), (4) large-scale physical modeling to produce accurate theoretical responses over targets of interest in environmental geophysics surveys, (5) rapid neural network interpretation at the field site, and (6) visualization of complex structures during the survey.

Research sponsored by the U.S. Department of Energy's Morgantown Energy Technology Center, under Contract No. DE-AC21-92MC29101 A001.

Introduction to EM System

Ground Penetrating Radar (GPR) has been shown to be a powerful tool for environmental investigations. Unfortunately, in many areas the attenuation of radar energy is much too great for radar to be effective. In the southwestern United States, for example, the depth of penetration of radar energy in basin-fill sediments is typically only one meter. In order to reliably obtain a usable depth of penetration for environmental investigations, it is necessary to use lower frequencies than are normally used in GPR investigations.

A high-frequency EM imaging system that overcomes the depth restrictions of ground penetrating radars has been developed for the frequency range 31 kHz to 32 MHz. The system is an extension of a previously developed imaging system which had a frequency range of 30 Hz to 30 kHz (Sternberg et al., 1991). The 31 kHz-to-32 MHz frequency range is necessary to provide high resolution over the range of depths that are of interest in environmental geophysics surveys.

High-Resolution Subsurface Electromagnetic Imaging System

Figure 1 shows a block diagram of the high-frequency EM imaging system. We currently transmit 11 frequencies sequentially in binary steps over the range 31 kHz to 32 MHz. The transmitter uses a sinusoidal signal supplied from the receiver via a fiber-optic cable. The signal is amplified by a power amplifier and sent to a narrow-band tuned transmitter coil. The tuning is automatically controlled with digital signals supplied via a second fiber-optic cable from the receiver. Fiber-optic cables are required to avoid interference from the transmitter directly into the receiver as would occur if a metallic wire were used between the transmitter and receiver.

The signals are received at transmitter/receiver separations of generally 2 to 8 meters using a tuned three-axis receiving coil. The signals from each axis are amplified by a preamplifier on the coil frame, conveyed to programmable filters and programmable amplifiers, and then digitized by a 100 MHz digitizing oscilloscope. The programmable filters, amplifiers and tuning are all controlled automatically via RS232 interface from an environmentally sealed and ruggedized computer. A waveform generator provides a calibration signal to the calibration coil located on the receiver coil. A second channel on the waveform generator provides the signal for the transmitter through the fiber-optic link. The digitizer and waveform generator are controlled via GPIB interface. The waveform generator and digitizer are precisely synchronized through a timing clock connection. The data from the receiver coil are signal-averaged, filtered and relayed to an interpretation workstation via an RF telemetry link. The interpretation workstation is located in a remote recording truck. The workstation uses neural networks (described in a later section) and displays the data for interpretation in the field.

The receiver modules are mounted on an all-terrain vehicle (ATV) (Figure 2a). The transmitter modules are mounted on a second ATV (Figure 2b). These ATVs are 6-wheel drive, amphibious vehicles, and can handle extremely rough terrain. The transmitter coil is located on a boom in front of one ATV. Ahead of or off to the side of the transmitter ATV is the receiver ATV with the receiver coil located on a boom extending out the back.

We have chosen to calculate ellipticity of the magnetic field from the observed magnetic field quantities. Hoversten (1981), in a comparison of time- and frequency-domain EM sounding techniques, showed that the frequency-domain ellipticity measurement is superior to any other frequency-domain or time-domain measurement for EM soundings. He also showed that "the ellipticity measurement provides smaller parameter standard errors than the time-domain data". "In addition, the model parameters arrived at through the least squares inverse are much less correlated with each other when ellipticity is used."

We define H_x as the component of the magnetic field in the direction along the survey line. H_y is in the direction perpendicular to the survey line, and H_z is the vertical component. If the transmitter is emitting a sinusoidally varying signal, the total magnetic field at the receiver will trace an ellipse in the XZ plane as a function of time. The ellipticity is defined as the ratio of the major to minor axes of the ellipse.

$$e = \left| \frac{H_2}{H_1} \right|$$

The ellipticity (e) can be determined directly from measurements of the relative magnitude and phase of the H_x and H_z fields.

$$e = \left| \frac{H_z \cos\alpha - H_x \sin\alpha}{H_z \sin\alpha + H_x \cos\alpha} \right|$$

where:

$$\tan(2\alpha) = \frac{2|H_z| \cos[\phi_z - \phi_x]}{1 - |H_z|^2}$$

and ϕ_z and ϕ_x are phases of vertical and horizontal components of the total field. The ellipticity measurement is discussed in Spies and Frischknecht (1991).

A number of novel features are included in the system design:

1) The calibration coil supplies a calibration signal to the receiver coil at the same time that the data are being collected. The calibration coil is coupled equally to all three axes of the receiver coil. It is parallel to the x-axis coil over one quadrant, then follows the y-axis coil for another quadrant, then the z-axis coil for a quadrant, and continues on around completing a closed loop. This allows equal calibration signals on all three receiver axes simultaneously with the data measurement. The cal-coil driver has a high output impedance so that the calibration coil does not interfere with the received signal. Four calibration frequencies are transmitted, which are offset slightly in frequency from the data frequency and surround the data frequency. The system response at the data frequency is then interpolated from these four nearby frequency responses. A key feature is that the calibration is performed simultaneously with the data acquisition, thereby preventing any errors due to drift in the system response, as well as greatly increasing the speed of data acquisition. This procedure is known as AFCAL (Adjacent Frequency CALibration). It is an adaptation of the HASCAL method (High-Accuracy Simultaneous CALibration) described by Sternberg and Nopper (1990).

The motivation for making as high an accuracy measurement as possible is based on previous publications which show that if we were able to obtain unlimited precision in our measurements, we would be able to uniquely determine the variation of conductivity with depth. For example, Fullager (1984) investigated horizontal-loop frequency soundings and demonstrated that these methods "are, in principle, imbued with unlimited resolving power". Unfortunately, only a small amount of error in the measured electromagnetic fields can lead to a large amount of error in the interpreted subsurface resistivity structure. Our goal is to obtain as high-accuracy measurements as possible.

A further requirement for obtaining high resolution is the need to obtain data over a large and densely sampled spatial area and at many frequencies. The entire data acquisition process in this system is totally automated. A complete sounding may be made in less than one minute. Therefore, dense spatial sampling can be obtained, as well as rapid surveys of large areas. The wide bandwidth of this system fulfills the need for many frequencies. Although we certainly will not obtain unlimited resolution,

we believe that the approach used in this system will provide greatly increased resolution over the current state-of-the-art.

(2) Both the transmitter and receiver coils have been optimized to obtain highly accurate data over a wide bandwidth. The coils consist of nested segments with increasing area and increasing number of turns in the outer coils for the lower frequencies. Therefore, adequate sensitivity is obtained over the entire bandwidth. A great deal of effort has gone into the design of these coils; in particular, each coil segment is decoupled from the surrounding nested coils and each coil segment has been optimized for a particular frequency range.

(3) The standard procedure for calculating ellipticity uses just H_z and H_x. However, for high-accuracy measurements we also record the H_y component perpendicular to the transmitter-receiver line and determine the ellipticity from all three vectors. This method uses a mathematical rotation of the observed magnetic fields to the major and minor axes of the ellipse and is described in Bak et al. (1993). Basically, this procedure first determines the azimuth of the electromagnetic field polarization and then determines the ellipticity of this azimuth. The mathematical rotation greatly speeds up the measurement of ellipticity in comparison with mechanically orienting the receiver coils, which is a very time-consuming process. The coil can simply be placed on the ground in any orientation and the rotation algorithm automatically rotates the field components to the major and minor axis values of the magnetic-field ellipse.

(4) This system records in a frequency range which includes effects from both conduction currents and displacement currents. It is difficult to obtain reliable numerical modeling calculations of theoretical responses to complex targets in this frequency range. We have adopted a different procedure which involves the use of full-size physical models. A large modeling tank has been constructed at our test site in Avra Valley, Arizona, west of the University of Arizona campus (Figure 3). The tank is 20 m long by 3 m deep by 6 m wide. The transmitter and receiver coils are kept stationary to avoid variations in response due to background effects. Various targets are then moved in the tank along a profile line under the coils. Repeated measurements are made with the targets at different depths, orientations, and with different types of targets. This allows us to generate a large number of theoretical model responses for data interpretation, including neural network training.

Introduction to Data Interpretation

The two fundamental components of the automated interpretation scheme are the neural networks and the data visualization shell. The data visualization shell provides the user interface to the neural networks, graphs of sounding curves, 1D forward modeling program, images of the data, and interpreted sections The only interaction the user has with the trained neural networks is the selection of the networks to use for the interpretation through the visualization shell.

The data interpretation system makes possible a first-pass, real-time interpretation with neural networks directly in the field. The acquired ellipticity data are transferred immediately after the acquisition computer finishes recording one sounding, via a wireless telemetry

system from the acquisition computer on the survey line to the interpretation computer in the truck. Each incoming sounding is automatically stored in the background of the program, and from then on is available for display and interpretation.

The user selects all the networks through which the data should be routed. Each network interpretation is passed to a 1D forward modeling program so the ellipticity curves can be compared to the measured data. The fit of each interpreted sounding to the field data is calculated as the mean-squared error for the 11 frequencies in each sounding. The user decides which network gives the best fit and the interpretation is plotted in a 2D section.

We have created 33 separate neural networks to do the 1D interpretation for either a 4 m or 8 m separation. Two additional networks classify data from 3D objects as target or background; if the data are classified as target, another network categorizes the response as low, moderate, or high conductivity.

Neural Network Interpretation

Ellipticity data are transferred from the field data acquisition computer via the RF telemetry link to the data interpretation computer housed in the field truck. The data interpretation consists of neural networks operating in mapping mode (1D) and object-location mode (3D). Our approach to the neural network processing is to divide the interpretation into many parts and use several small networks. The interpretation system currently uses two different transmitter-receiver offsets of 8m and 4m. Thirty-three separate networks are used for each offset for a total of 66 networks. Nearly 280,000 models were used for training. Two network paradigms were used for training, a radial basis function algorithm and a modular neural network algorithm. The networks perform parameter estimation and classification. Each network is capable of producing an interpretation in a few milliseconds on a 486 PC.

Mapping Mode. In mapping mode we have two categories of networks: halfspace nets and layered-earth nets. The piecewise apparent resistivity nets, 8 for each separation, fit a halfspace model to each frequency triplet in a sounding. The apparent resistivity nets use all 11 frequencies to fit one halfspace model. The main difference between the two is that if there is a frequency dependence for conductivity, the apparent resistivity nets will do a better job of fitting the data. The halfspace networks are trained on models ranging from 1 to 10,000 ohm meters using a radial basis function algorithm.

The layered-earth networks interpret two-layer models. Modular neural networks are used for the layered-earth interpretations. Many different algorithms were tried but only the modular network could produce accurate enough results for both thickness and resistivity. The estimated model parameters for each selected net are input to a forward-modeling code and ellipticity curves are generated for each. The ellipticity curves are plotted along with the field data and the mean-squared error is calculated for each interpretation versus the field data. The user can then select the best-fit model and use that for the interpretation.

The layered-earth networks interpret two-layer models. We fix the thickness of the layer and estimate the resistivity and dielectric constant. A separate neural network is used for each thickness increment. The thinnest layer is 20 cm. For an 8 m separation, the thickest layer is 4.8 m; for a 4 m separation, the thickest layer is 2.4 m. We use an increment of 20 cm for the

layer thickness. Preliminary results at an 8 m separation indicate that we have more difficulty resolving layers less than 1 m thick. For layers more than 1 m thick, the resistivity estimates are an average within 95% of the desired value. The dielectric constant for the top layer is always much better resolved than that of the lower half space. The dielectric constant is better resolved for resistive models than conductive ones. We cannot resolve the dielectric constant for resistivities below 50 ohm-m.

Object-Location Mode. We have a preliminary object-location mode set of neural networks based on data collected over the Cold Test Pit (CTP) at the Idaho National Engineering Laboratory. The networks are trained using field data rather than modeled data. The first network classifies sounding curves from each survey station as representing background or target. Figure 4 shows sounding curves for the 32 kHz to 1 MHz frequency range for background (bottom graph) and over the center of the CTP (top graph) for several survey lines.

We used 134 soundings over the CTP for the target vs. background classification. All 11 frequencies were used as input. The data were quite easily classified as background or target. The network was tested on an additional 34 soundings over the CTP. Only one station in the training set was misclassified as waste when it was labeled as background and it was on the edge of the waste pit. One station in the test site was weakly classified as waste when it was labeled background. The labeling of stations as waste or background was based on a map of the CTP provided to us by INEL personnel. We have no information on the accuracy of this map. We also do not yet know how site-specific this classification is. Classification results are shown in Figure 7.

We developed a second neural network that further classified data points identified as waste according to its type, based on the CTP map. The categories of waste were: drums, boxes, crushed drums, and pipes. We used 137 samples for training (including background samples). Seven samples were used for testing. In the training set, five stations labeled as drums were misclassified as background out of the 137 training samples; two stations out of the 7 test samples over boxes were misclassified as background according to the map. The classification results are shown in Figure 8.

This labeled classification procedure indicates areas of similar signatures rather than waste type itself. If the ellipticity sounding curves were not similar in each of the categories, then the classification could not be accomplished. Features other than waste type, however, could account for the similarities (such as depth, fill material, cap characteristics) and perhaps other properties. More research needs to be done on signatures over different types of waste. A simpler classification based on relative conductivity may prove more robust.

Data Visualization Software

The Ellipticity Data Interpretation System (EDIS) was developed based on the Interactive Data Language (IDL) graphics software for WINDOWS on a personal computer (PC). EDIS goes far beyond the built-in routines of IDL; it also uses the IDL capabilities of interacting with DOS based programs, WINDOWS based programs and dynamic link libraries (DLL).

Display capabilities in EDIS are for sounding curves, interpreted sections, and raw ellipticity data. The user may select up to twelve sounding curves to display at one time. The

difference between the last two selected curves is automatically displayed on a graph below the sounding curves. Interpreted data are displayed in 2D sections that show the color-coded resistivities. The y-axis of the sections indicates the thicknesses of the interpreted layers. Several sections can be displayed at one time for other offsets or lines. Raw ellipticity data can be displayed versus frequency number or skin depth. Future enhancements to the software will include more image processing capability for the ellipticity images, 3D block models of the ellipticity and interpreted data, file format transformations, improved plotting capability, preprocessing algorithms for 3D objects, and inclusion of tilt angle.

The field data can be displayed and compared to previous stations. Quality control is performed by comparing combined neural network and forward-modeling results with the field data. After deciding on a particular neural network for the interpretation of a specific station the neural network results will be written to disk and can be used to build up a resistivity or ellipticity section interactively. Several printing options and utilities are also available within EDIS.

Future enhancements to the software will include more image processing capability for the ellipticity images, 3D block models of the ellipticity and interpreted data, file format transformations, improved plotting capability, and preprocessing algorithms for 3D objects.

Field Survey

We conducted a survey at the Idaho National Engineering Laboratory (INEL) near Idaho Falls, Idaho from November 28 to December 1, 1995. The survey was run over an area known as the Cold Test Pit (CTP). This site is a simulated waste pit that is representative of the waste pits at INEL and elsewhere in the DOE complex. Figure 5 shows a map of the CTP and the locations of our survey lines. We collected data at approximately 300 stations in 3 days of surveying. Typical data collection times were about one minute to acquire data and two minutes to move and set up at the next station.

Figure 6 shows a representative cross section derived from the piecewise apparent resistivity neural networks. A 1 m thick top layer is very prominent. The boundaries of the waste pit are clearly delimited and correspond to the edges of the waste in Figure 5. The bottom of the waste is not resolved, nor is any detail within the pit.

Figure 7 shows a neural network classification of the background versus waste. Background is indicated by white and light gray pixels. Waste is indicated by black and dark gray pixels. Figure 8 shows a neural network classification of various types of waste. See the section of this paper on ‘Neural Network Interpretation, Object Location Mode’ for more information on the procedures used for these classifications.

Acknowledgments

This research was sponsored by the U.S. Department of Energy’s Morgantown Energy Technology Center, under Contract No. DE-AC21-92MC29101 A001. The LASI high-resolution EM systems have evolved over many years. Support for this development has included: Electric Power Research Institute, The Copper Research Center, U.S. Geological

Survey, U.S. Bureau of Mines, Department of Energy, U.S. Army, and University of Arizona.

References

Bak, N.H., 1992, Sternberg, B.K., Dvorak, S.L., and Thomas, S.J., 1993, Rapid, high-accuracy electromagnetic soundings using a novel four-axis coil to measure magnetic field ellipticity, J. Applied Geophysics, 30, 235-245.

Fullager, P.K., 1984, A uniqueness theorem for horizontal loop electromagnetic frequency soundings, Geophys. J. R. Astr. Soc., 559-566.

Hoversten, G.M., 1981, A comparison of time and frequency domain EM sounding techniques, Ph.D. Thesis, Univ. of California, Berkeley, 169 p.

Spies, B.R., and Frischknecht, F.C., 1991, Electromagnetic sounding, in: Electromagnetic Methods in Applied Geophysics, Vol. 2, M.N. Nabighian, ed., 285-425.

Sternberg, B.K., and Nopper, R.W., 1990, High-accuracy simultaneous calibration of signal measuring systems, Meas. Sci. Technol., 1, 225-230.

Sternberg, B.K., Thomas, S.J., Bak, N.H., and Poulton, M.M., 1991, High-resolution electro-magnetic imaging of subsurface contaminant plumes, EPRI, RP-2485-11, Palo Alto, CA.

Figure 1. Block diagram of high-resolution ellipticity system.

Figure 2a. Photograph of the amphibious all-terrain field vehicle with the computer enclosure and receiver-module enclosure mounted on it.

Figure 2b. Photograph of the transmitter all-terrain vehicle with the transmitting antenna suspended from the boom in front of the ATV.

Figure 3. Photograph of the completed physical modeling facility prior to filling with fluid. A trolley with targets suspended at various depths is moved down the length of the tank during the measurements.

Figure 4. Ellipticity sounding curves over background soil (bottom graph) and waste (top graph) for survey lines at the Cold Test Pit (CTP).

Figure 5. Map showing the Idaho National Engineering Laboratory (INEL) Cold Test Pit (CTP) and the nine lines surveyed by the LASI ellipticity survey.

Figure 6. Resisitivity depth sections created from piecewise apparent neural network interpretations for the lines 2.5S and 7.5S at the INEL CTP (8m transmitter-receiver spacing).

Figure 7. Classification map of waste versus background from a neural network. Values near -1 represent background, values near +1 represent waste.

Figure 8. Classification map of waste type from a neural network.

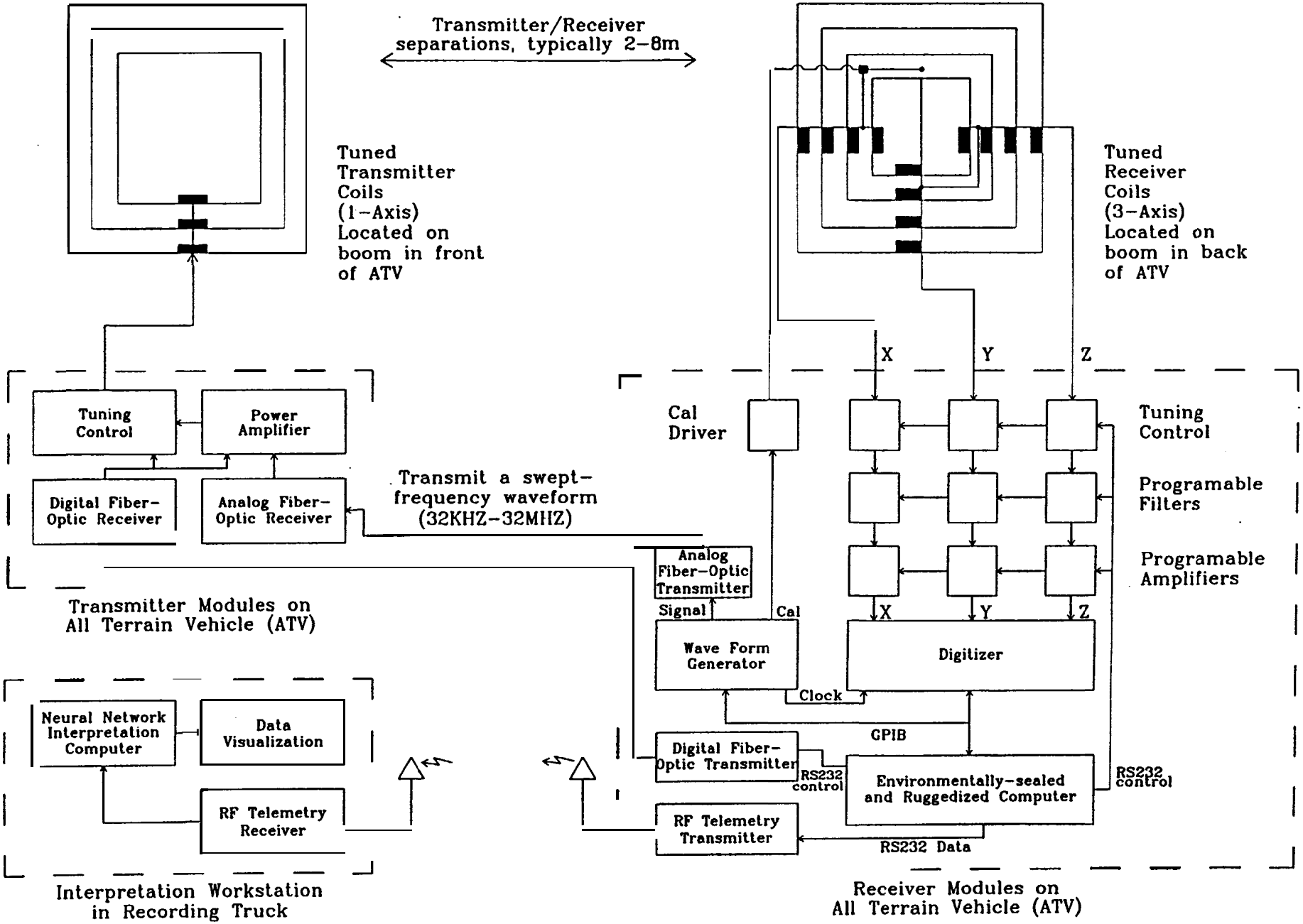

Figure 1. Block diagram of high-resolution ellipticity system.

Figure 2a. Photograph of the amphibious all-terrain field vehicle with the computer enclosure and receiver-module enclosure mounted on it.

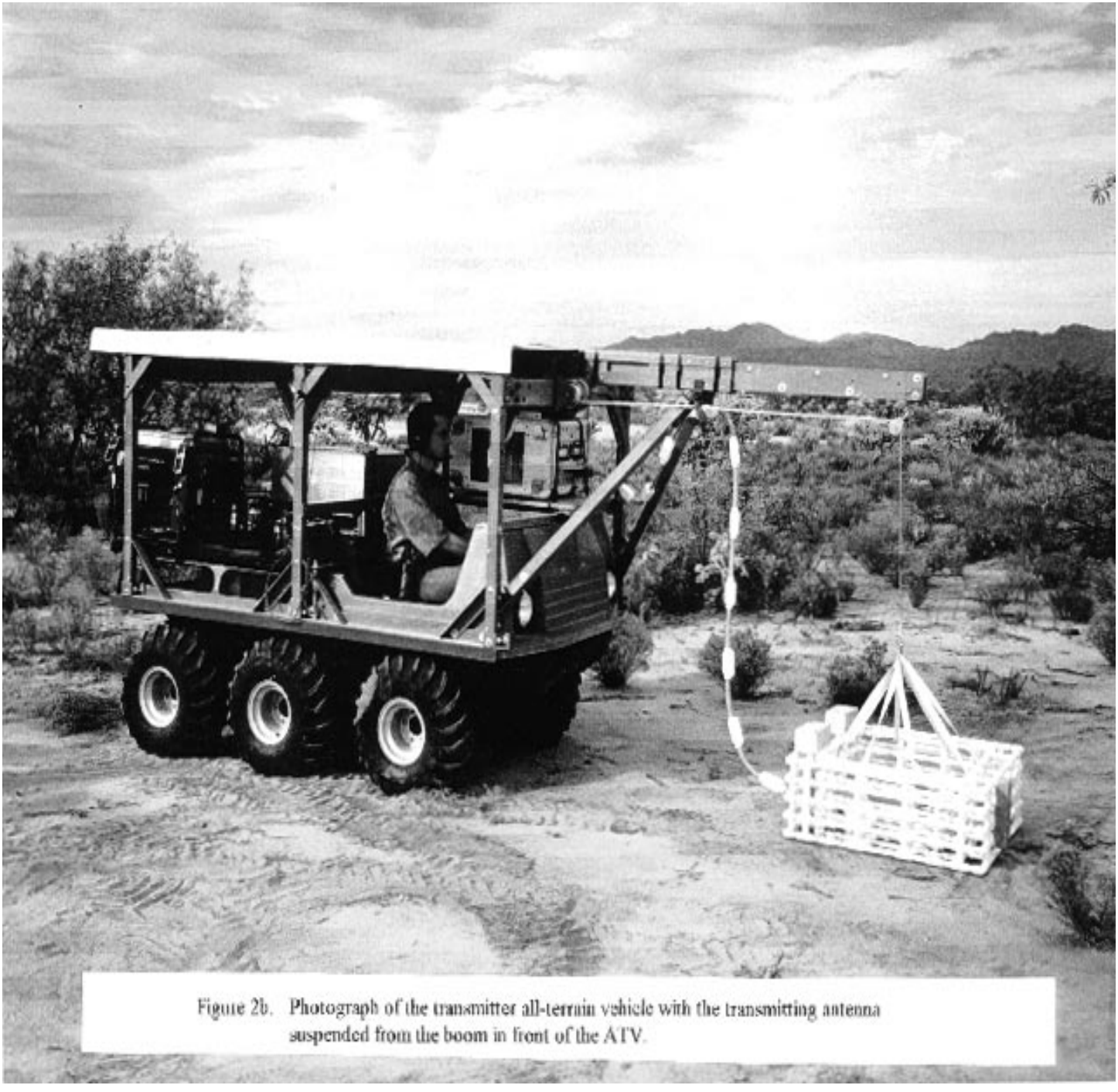

Figure 2b. Photograph of the transmitter all-terrain vehicle with the transmitting antenna suspended from the boom in front of the ATV.

Figure 3. Photograph of the physical modeling facility during experiments to determine the ellipticity response to various objects (e.g. barrels, pipes, and sheets). The walls of this tank were covered with shotcrete containing fiberglass for added strength. There is no metal reinforcing rod used in this physical modeling tank. A trolley (shown in front of the transmitter ATV), with targets suspended at various depths, is moved down the length of the tank during the measurements.

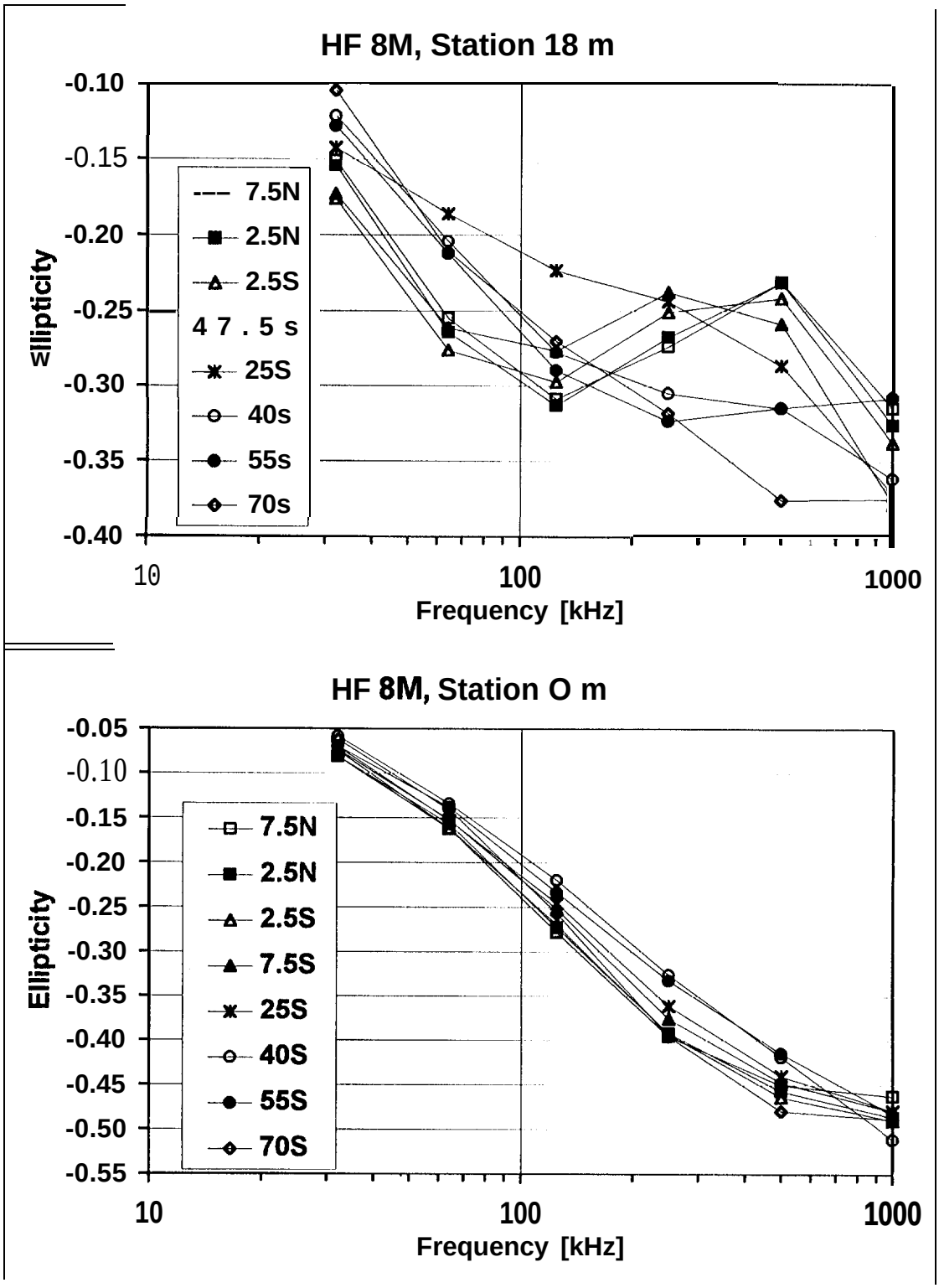

Figure 4 Ellipticity sounding curves over background soil (bottom graph) and waste (top graph) for survey lines at the Cold Test Pit (CTP)

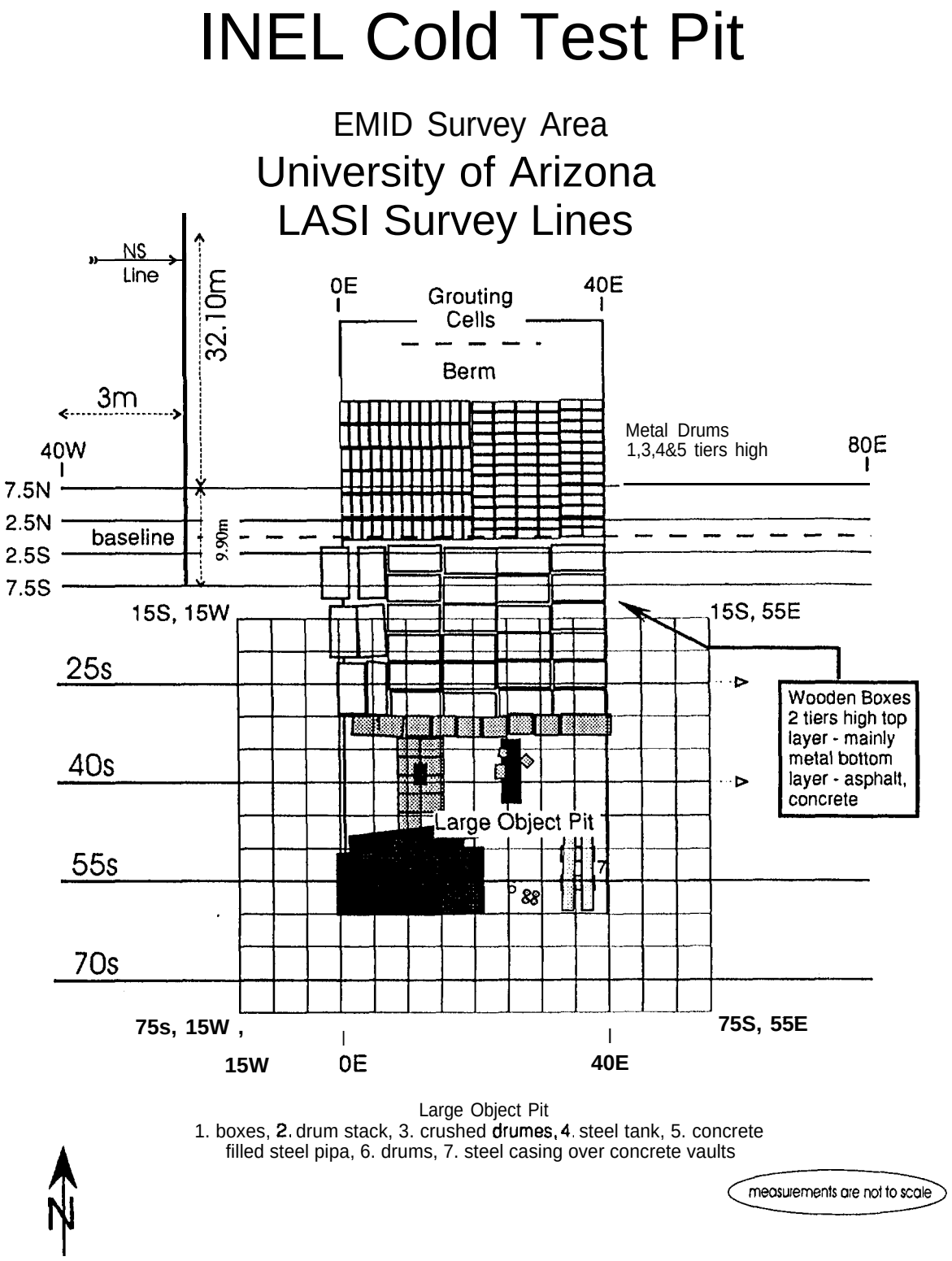

Figure 5. Map showing the Idaho National Engineering Laboratory (INEL) Cold Test Pit (CTP) and the nine lines surveyed by the LASI ellipticity survey.

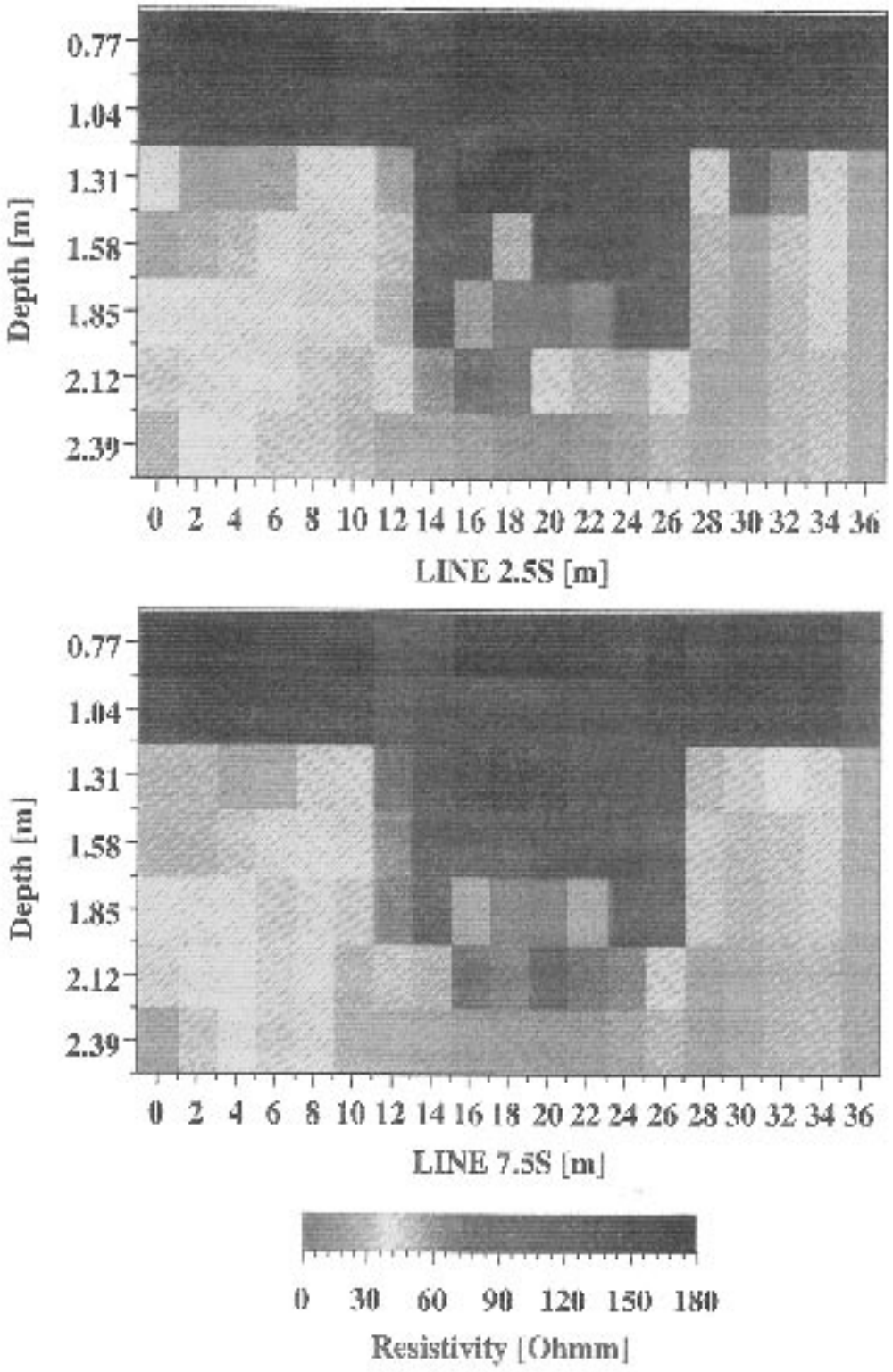

Figure 6. Resistivity depth sections created from piecewise apparent neural network interpretations for the lines 2.5S and 7.5S at the INEL CTP (8m transmitter-receiver spacing).

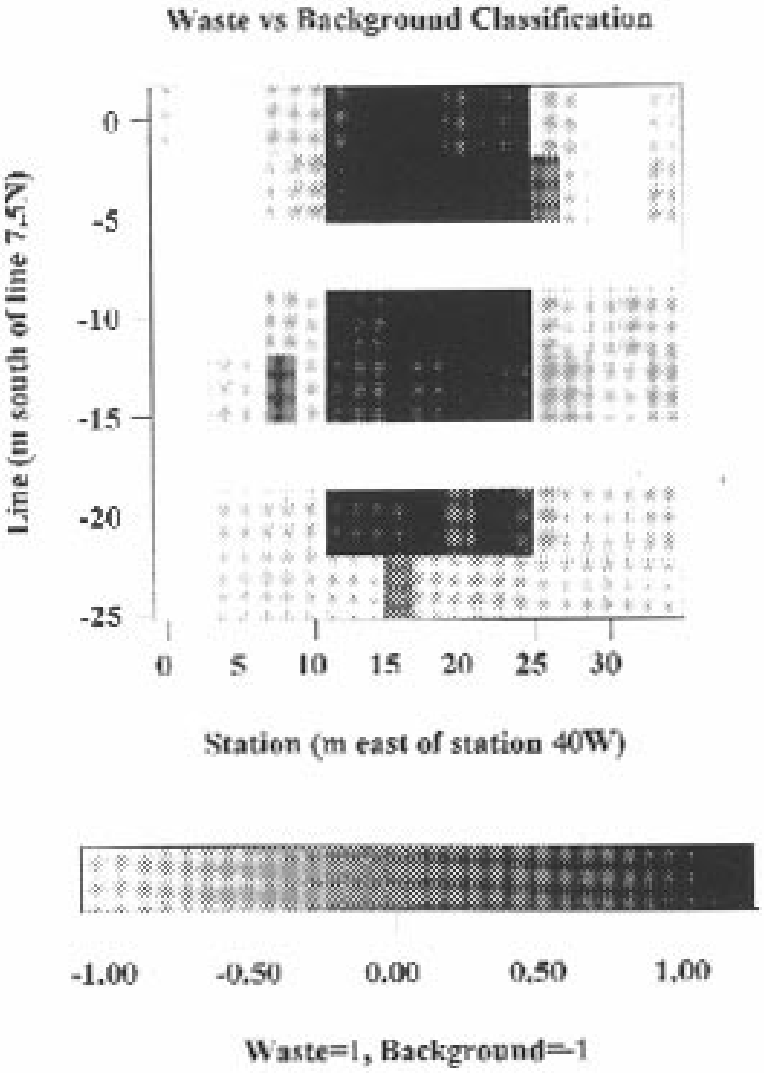

Figure 7. Classification map of waste versus background from a neural network. Values near -1 represent background, values near +1 represent waste.

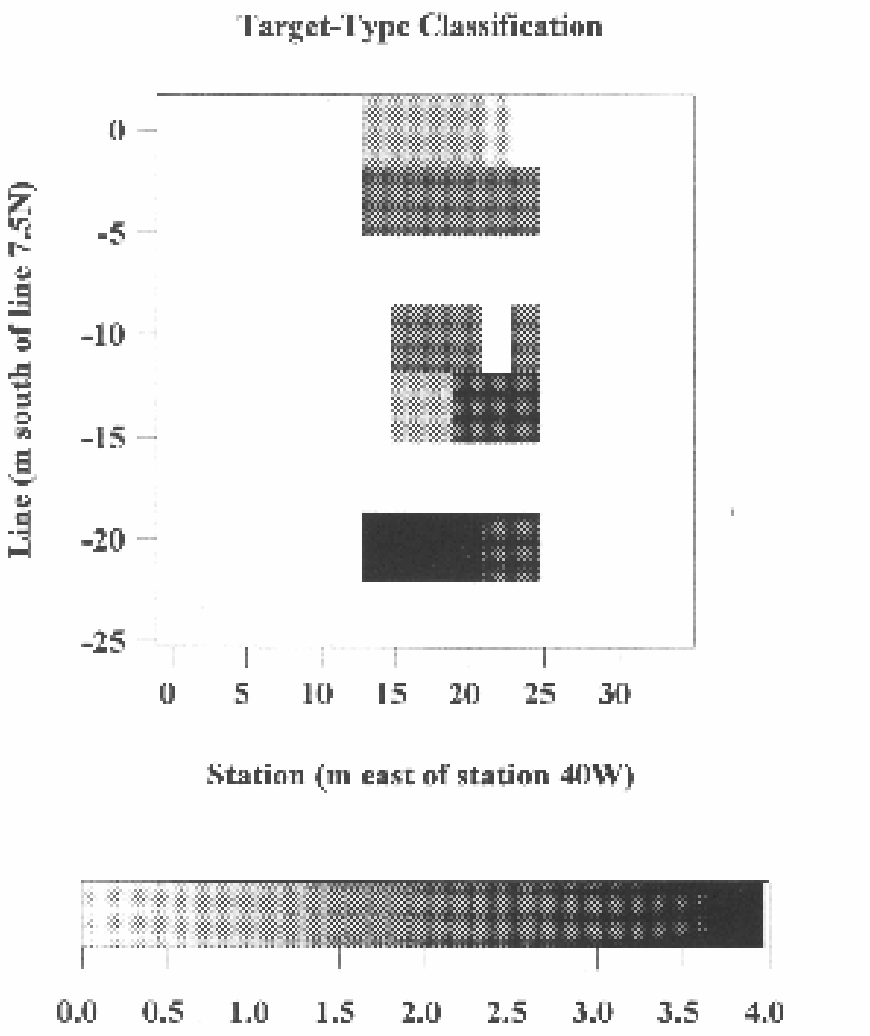

Figure 8. Classification map of waste type from a neural network.